Available online at www.sciencedirect.com
SCIENCE DIRECT®
Surface Science 589 (2005) 129–138
SURFACE SCIENCE
www.elsevier.com/locate/susc

Single electron tunneling and manipulation of nanoparticles on surfaces at room temperature

Guohua Yang [a], Li Tan [a], Yiyun Yang [b], Shaowei Chen [b], Gang-Yu Liu [a,*]

[a] *Department of Chemistry, University of California, One Shields Avenue, Davis, CA 95616, USA*
[b] *Department of Chemistry and Biochemistry, University of California, Santa Cruz, CA 95064, USA*

Received 7 October 2004; accepted for publication 25 May 2005
Available online 27 June 2005

Abstract

This article focuses on surfaces containing nanoparticles and self-assembled monolayers (SAMs). These surfaces provide a simple and reliable platform for measurements of single electron tunneling (SET) properties of metal nanoparticles at room temperature. This approach of interfacial chemistry allows for the elimination of lateral motion of the individual nanoparticles during electronic property studies. The scanning tunneling microscopy (STM) in ultra-high vacuum is used as an accurate and reproducible probe for imaging and *I–V* characterization of individual or aggregated Au nanoparticles, revealing a large Coulomb gap (1.0 eV) and fine Coulomb staircases (0.2–0.3 eV) at room temperature. The surrounding decanethiol SAM provides an ideal reference for the imaging and *I–V* measurements of nanoparticles. These measurements provide a quantitative guide for regulating current and voltage, at which individual Au nanoparticles may be detached and manipulated with the STM tip.

Keywords: Single electron effects; Coulomb blockade; Coulomb staircases; Nanoparticles; Molecular electronics; Scanning tunneling microscopy

1. Introduction

Surfaces with novel nanostructures have many applications in fields of nanoelectronics [1,2], biological microelectromechanical system (BioMEMs) [3], as well as molecular electronics [4,5]. One of the challenges of nanotechnology lies in the ability to measure material properties in those nanostructures. This article provides a simple and reliable protocol used to measure single electron tunneling (SET) properties of a special nanostructure, that is, metal nanoparticles, at room temperature. SET behavior has been reported for small metallic particles, especially at cryogenic temperatures [6–10].

* Corresponding author. Tel.: +1 530 754 9678; fax: +1 530 752 8995.
E-mail address: gyliu@ucdavis.edu (G.-Y. Liu).

0039-6028/$ - see front matter © 2005 Elsevier B.V. All rights reserved.
doi:10.1016/j.susc.2005.05.061

The signature of SET is the appearance of both the Coulomb blockade and Coulomb staircases [11]. SET has been recognized as the basis of future single-electron devices and as a probe for measuring electronic properties, i.e., conductance and capacitance, among interfaces or molecules on the nanometer scale [12–15]. Further development of SET based nanodevices requires (i) the knowledge and ability to design a SET with desired properties at room temperature; (ii) a reliable test platform to characterize device components such as nanoparticles (NPs), surroundings, and electrodes; (iii) an advanced methodology to tune the electronic properties in the device; and (iv) reliable and reproducible methods to engineer stable devices with single NP precision.

Much progress has been made in the past decade in all, especially the first three, areas of research. We have learned that, in order to observe both the Coulomb blockade and staircases, two necessary conditions have to be satisfied [11]. First, the charging energy, $E_c = e^2/2C$, determined by the addition of one electron to the metal particle with capacitance C, must exceed the thermal energy k_BT. If this condition is not fulfilled, thermally activated electrons will overcome the Coulomb barrier and lead to a non-zero tunneling current. Second, the electric contacts to the particles should have tunneling resistances larger than the quantum resistance, $h/4e^2$ ($\sim$6.5 kΩ), in order to suppress quantum fluctuations of the electron charge. Typically, only nanometer-sized particles with a capacitance on the order of 10^{-18} F satisfy these conditions and exhibit SET effects at room temperature [11].

Scanning tunneling microscopy (STM) and spectroscopy (STS) have proven to be an accurate test platform for SET and conductance/capacitance measurements [6–8,10,12,16,17]. STM not only is able to image NPs with high resolution, but also can perform current–distance (I–Z) and current–voltage (I–V) spectroscopy measurements. In I–V measurements, the STM multiple junctions, i.e., tip/passivation layer/NP/passivation layer/electrode, can be modeled using an equivalent circuit of a double barrier tunneling junction (DBJT), as shown in Fig. 1(a) and (b). For successful and reliable STM experiments, NPs must be immobilized on electrodes. Andres et al. first introduced an immobilization protocol for bare Au-NPs using a dithiol self-assembled monolayer (SAM) on a Au(1 1 1) substrate [12]. Room temperature Coulomb blockade and Coulomb staircases are observed using these immobilized Au-NPs [12]. Harrell et al. modified and improved this procedure by adsorbing alkane thiols on Au-NPs to minimize aggregation and to simplify sample preparation [7,8]. This approach's limitation is that the interaction between the STM tip and NPs often leads to lateral displacement of the particles, manifested as streaking in the STM images. Thus, SET measurements could only be conducted on aggregated particles [7].

The electronic properties in SET may be tuned at cryogenic temperatures, as reported by Wang et al., by varying the size of NPs (changing R_1 and C_1) and the STM tip–NP distance (changing R_2 and C_2) [10]. Generally, the variable core size of these particles allows the Coulomb blockade gap to be tuned from 50 to 1000 meV [10]. It is difficult to extend this approach to room temperature due to lateral movement of NPs as a result of weak particle–surface interactions. Such lateral instability makes parking the tip precisely on the NP surface difficult, raising doubts about the reproducibility of the I–V spectroscopic measurements at room temperature.

Since I–V measurements in aggregated NPs complicate the extraction of junction parameters [11], better protocol needs to be developed in order to immobilize NPs separately for reliable molecular conductance measurements. In addition, the passivated NPs must have a strong binding to the substrate to prevent lateral motion during the scan at room temperature, and thus have a well-controlled molecular orientation in junction 1. Furthermore, advanced methodology needs to be developed to position and engineer SET based devices with single particle precision. This article intends to address aforementioned issues by introducing a new modification to previously reported NP immobilization protocols. UHV-STM studies demonstrate that NPs in individual and aggregated forms can sustain the tip–NP interactions during STM imaging as well as spectroscopy studies at room temperature. In addition, NPs can be

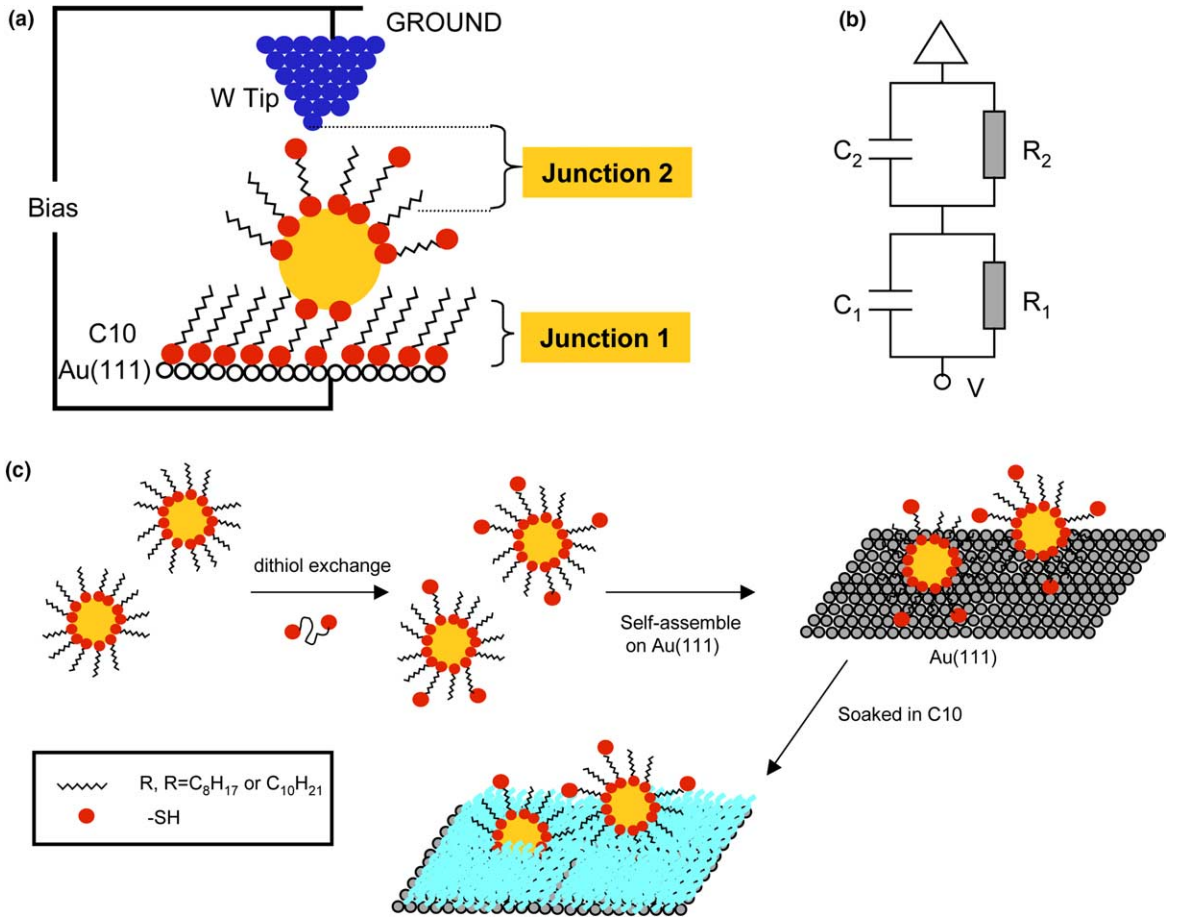

Fig. 1. (a) A schematic of DBTJ device formed by an STM tip, a ligand-stabilized gold particle, and a Au substrate. (b) Corresponding equivalent circuit for the DBTJ. (c) A scheme of particle immobilization procedures.

moved from adsorption sites in a controlled manner and with a single particle precision.

2. Experimental

SAM covered Au-NPs were synthesized using the previously published procedures [18,19]. Briefly, gold NPs covered by n-octanethiolate ($C_8H_{17}SH$, supplied by Aldrich) were synthesized by the Brust reaction [19]. These particles were then subject to size fractionation and thermal annealing to reduce size dispersity. Transmission electron microscopy (TEM) imaging has shown a core diameter of approximately 1.5 nm (with a dispersity of about 20%) for NPs selected for this investigation [19]. NPs were further chemically functionalized with 1,8-octanedithiol through an exchange reaction [18]. At the end of the reaction, excess octanedithiol ligands were removed by repeated extraction with methanol. The final concentration of octanedithiol on the particle surface was about 50%, that is, on average, about 26 ligands each for octanethiol and octanedithiol on the Au core surface [18]. The resulting surface-active particles were kept in hexane prior to the STM experiments.

Au(1 1 1) surfaces, that is, the electrodes used for NP immobilization, were prepared following established procedures [20,21]. Freshly cleaved

mica was heated to 350 °C in vacuum (10^{-7} Torr range) before pure gold (Alfa Aesar, 99.99%) was thermally evaporated onto it. The gold films, ~200 nm in thickness, were cooled to room temperature before being taken out of the chamber. The STM operates under an ultra-high vacuum (UHV) (RHK Technology) [20,21], which is equipped with a fast entry load-lock for the transfer of the samples and tips under a base pressure of about 3×10^{-10} Torr. The STM tips were made from a 0.010 inch tungsten wire (California Fine Wire) by electrochemical etching in a 3 M sodium hydroxide solution [20,21].

3. Results and discussion

3.1. Nanoparticle immobilization and STM imaging

The NP immobilization protocol includes the following procedures as illustrated in Fig. 1(c). First the gold thin films were taken out of the vacuum chamber and then hydrogen flamed to improve the surface texture. The flamed films were subsequently immersed in the 0.05 mg/ml Au-NP suspension for 24 h. Then, the sample was immediately dipped into a 0.1 mM solution of decanethiol ($C_{10}H_{21}SH$, supplied by Aldrich) in ethanol for 1 h, followed by rinsing with ethanol and hexane. Finally, the sample was transferred to the UHV-STM system for imaging and *I–V* measurements. In this protocol, the Au-NPs (diameter ~ 1.5 nm) are self-assembled onto the Au(1 1 1) surfaces via S–Au chemisorption and the rest of the Au(1 1 1) surface is immediately passivated by alkanethiol SAMs. This approach utilizes the dithiol molecules ($C_8H_{18}S_2$) to immobilize Au-NPs on Au(1 1 1) surfaces. However, such linkage alone cannot effectively prevent the lateral movement of NPs during the scan [8]. This lateral instability is further alleviated by the introduction of the surrounding decanethiol SAM. Since alkanethiols form closely packed and ordered structures on Au(1 1 1) [20,21], this method assures the standing up and all-trans conformation of dithiol and alkanethiols under Au-NPs, which further stabilizes junction 1. In addition, the STM imaging and STS study of decanethiol molecules are well established [20,21], which provides an internal calibration for both imaging and spectroscopy studies of Au-NPs.

Fig. 2(a) demonstrates the stability and separation of NPs prepared using this method, where the interparticle distance ranges from 5 to 20 nm. As a reference, the corresponding decanethiol matrix surrounding the particles is imaged and shown in Fig. 2(b), in which the characteristic ($\sqrt{3} \times \sqrt{3}$)R30° structure of decanethiol SAMs is clearly visible [21,22]. The periodicity of decanethiol SAMs serve as a guide for determining the dimension of NPs, while the *I–V* characteristic of deca-

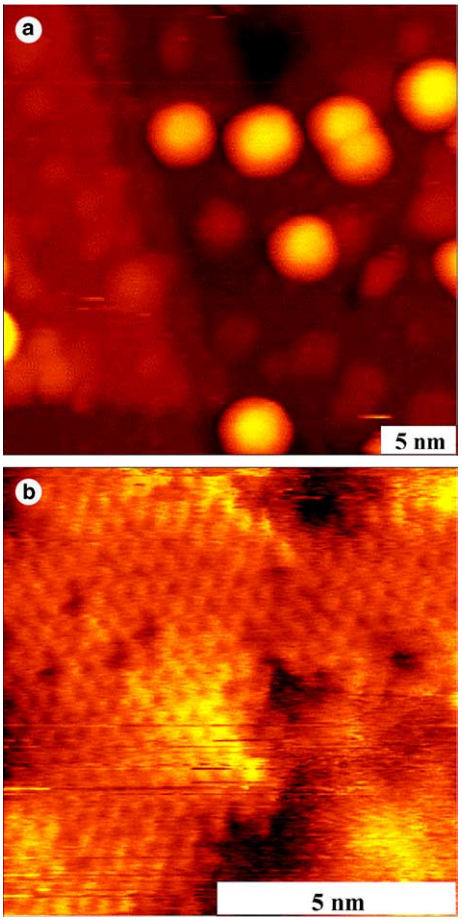

Fig. 2. (a) A topographic image of Au nanoparticles upon immobilization on gold electrode, acquired at 1.0 V and 10 pA. (b) A topography of decanethiol SAM surrounding individual Au particles, taken at 1.0 V and 30 pA.

nethiol provides an excellent reference for investigating NPs' electronic properties.

3.2. Coulomb blockade and staircases revealed by I–V spectroscopy study

The stable, high-resolution images enable the selection of NPs for spectroscopy studies at room temperature. It is worthwhile to note that consistent tip–NP distance is the basis for a reliable and reproducible I–V characterization, as the R_2 and C_2 of junction 2 varies as a function of tip–NP distance. Following our previous study on a model of molecular electronics [20], we use I–Z measurements as the guide to consistently park STM tips. The STM tip is firstly parked over an individual NP and the corresponding setpoint of 1.0 V and 39 pA is chosen as the reference ($z = 0$ is designated at this point). Subsequently, the I–Z measurement was acquired as shown in Fig. 3(a), where the tunneling current increases exponentially as tip approaching the NP. A kink point occurred during approaching, indicating the tip–SAM contact and a vertical spacing of 1.0 Å between the tip and the top of the passivated Au-NP at the reference point [20]. When the tunneling current is tuned from 18 to 66 pA under the same bias of 1.0 V, that is, when the tip approaches closer to the NP, with the assumption of a logarithmic relationship ($I/V = Ae^{-kz}$) between the tunneling conductance (I–V) and the tunneling gap z, the corresponding tip–NP distance can be calculated to be 1.5 and 0.7 Å, respectively. The tip–NP separation determined by such manner was used to consistently park the tip prior to I–V measurements. Similarly, Fig. 3(b) shows the I–Z spectrum of a decanethiol matrix next to one isolated individual NP.

Current vs. voltage (I–V) spectra in Fig. 4(a) clearly show that the tunneling current increases with the tip–particle distance reduction. At room temperature, both Coulomb blockade and staircase were observed, for both individual and aggregated Au-NPs, as shown in Fig. 4(a) and (b), respectively. Zero conduction region was measured from −0.45 to +0.45 V, which indicates that no electrons were transported through the junctions, i.e., Coulomb blockade. In contrast, tunneling current was always measurable throughout the biasing range for the surrounding decanethiol area (see Fig. 4(c)). The I–V traces in Fig. 4(c) are linear with small slopes at small voltages, and the slopes increases with increasing voltage. The slopes for alkanethiols never reach zero, i.e., no Coulomb blockade is observed. This observation is consistent with previous studies of alkanethiol SAMs [23–25]. The appearance of the Coulomb blockade in Fig. 4(b) of aggregated Au-NPs reveals sufficient electric isolation among neighboring particles due to the thiol modification. Such isolation was difficult to achieve in the past, e.g., in Co clusters supported by high dielectric Al_2O_3 film [17]. This electric isolation among neighboring NPs is especially desired in the construction of single-electron devices, e.g., floating gate devices. It is important to note that these I–V curves were repeatedly taken

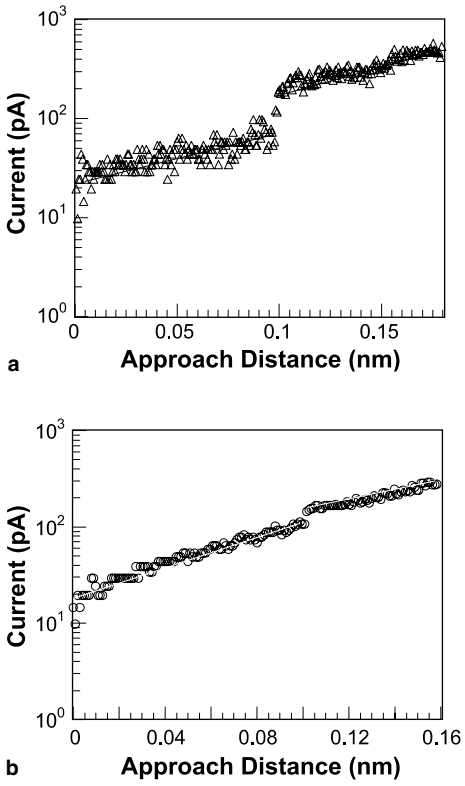

Fig. 3. An I–Z spectrum on (a) an individual Au nanoparticle (setpoint 1.0 V and 39 pA) and (b) decanethiol matrix (setpoint 1.0 V and 30 pA).

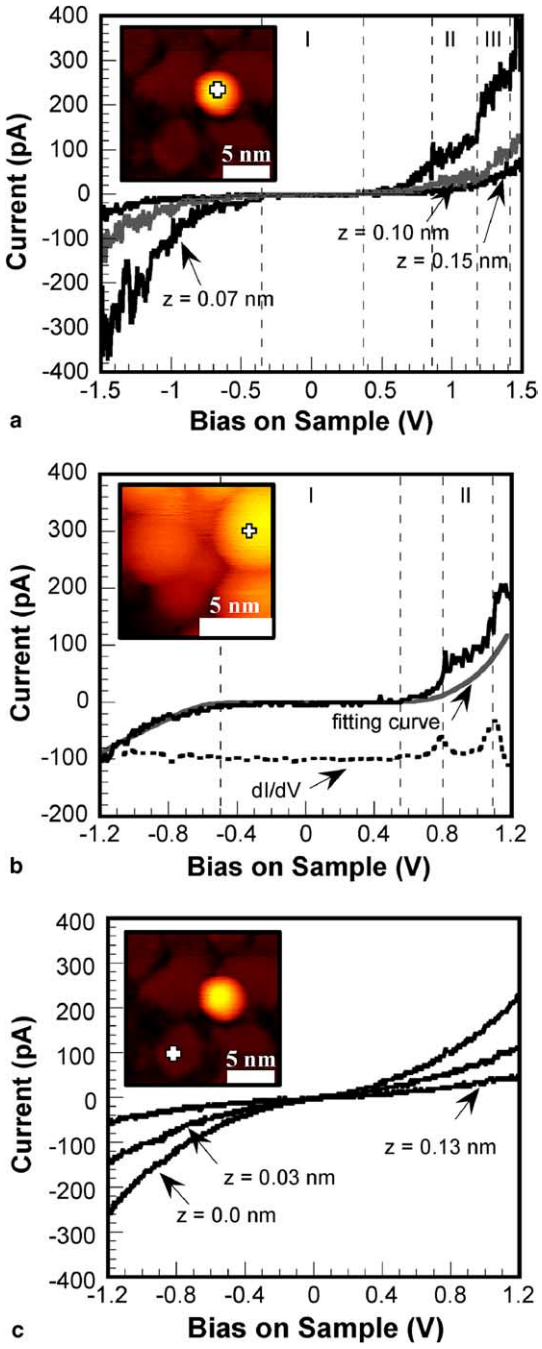

Fig. 4. Scanning tunneling spectroscopy of Au nanoparticles at room temperature: (a) I–V measurements above the nanoparticle indicated in the insert at defined tip–particle distances (z). (b) An I–V curve above one of the nanoparticles among the arrays (see insert). The digital derivative of $\mathrm{d}I/\mathrm{d}V$ is deduced and shown below the I–V curve. The initial setpoint is 1.0 V and 80 pA. (c) I–V spectra of decanethiol SAM in the surrounding. Initial setpoints are 1.0 V and 120, 80, and 20 pA, respectively (from top to bottom), which corresponds to a tip–particle distance of 0.00, 0.03, and 1.30 nm, respectively. Coulomb blockade in region I and staircases in regions II and III are also indicated in each I–V spectrum.

over the NPs without introducing conformational changes or lateral movements.

While Coulomb staircases usually exist as equidistant current steps similar to the Coulomb blockade for large size NPs (diameter > 4 nm) [10], the situation is different in the present system, where the particle core is ~1.5 nm. Nanoparticle's from the STM image in Fig. 4 is ~4.1 nm, if we consider that octanethiol and 1,8-octanedithiol ligands have a chain length of approximately 1.1 nm and an average core size of 1.5 nm, the lateral dimensions of the individual nanoparticles appear to be reasonable. Inasmuch, the I–V curves in Fig. 4(a) and (b), along with the digital derivative of $\mathrm{d}I/\mathrm{d}V$ curve in Fig. 4(b), have an uneven spacing between the adjacent current steps, with a width of 1 eV at the zero conductance region and a spacing of 0.2–0.3 eV for the other current steps. Furthermore, the I–V spectra share an asymmetric shape between the current in negative and positive biases, suggesting the existence of a non-zero value of fractional charge (Q_0) on the NP. It has been suggested that the zero conductance region is due to the additional charging energy obtained from quantum size confinement and narrow spacing within the discrete energy levels of electrons in the Au particles [10]. Since the mean spacing of energy levels within a Au-NP is expected to be only 0.07 eV ($\sim 3k_{\mathrm{B}}T$), a plausible explanation associated with the occurrence of 0.2–0.3 eV may be due to the further spatial confinement from the chemisorption of S atoms on the Au particle surface [10].

3.3. Extracting electronic properties of junctions

Using the DBTJ model, one can quantify the electronic properties, e.g., resistance and capacitance, by curve fitting the equivalent circuit, as summarized in Table 1. For a given passivated Au-NP, the capacitance C_1 is fixed and the variation of tip–particle distance with different setpoint currents can change C_2. By treating these particles as spheres, we estimate an overall geometric capacitance [16] ($C_t = C_1 + C_2$) of the NPs as $C_t = 2\pi d\varepsilon_0\varepsilon = 2.1 \times 10^{-19}$ F, where a particle diameter d of 1.5 nm and a dielectric constant of $\varepsilon = 2.5$ for alkanethiol SAMs are assumed [25]. Since the electrostatic charging energy (E_{c}) of the system estimated from the blockade width is around 0.45 eV, the corresponding tunneling capacitance $C_t = e^2/2E_{\mathrm{c}} = 1.8 \times 10^{-19}$ F can be calculated, and this value agrees well with the geometric estimation.

In addition, since the STM tip is at a fixed distance with respect to the center of NPs, $R_2C_2 \gg R_1C_1$. From the analytical expression derived by Hanna and Tinkham [26], the slope on the steps (n_0 constant) in the I–V curve is given by C_1/R_2C_t and the current jump (where $n_0 \rightarrow n_0 + 1$) is equal to $e\ R_2C_t$. These two data, i.e., a slope of 30 pA/0.4 V and a current jump of 100 pA, can be extracted from Fig. 4(b), and $R_2 \approx 8.9$ GΩ and $C_1 \approx 1.2 \times 10^{-19}$ F can be then calculated. C_2 can be calculated from C_t and C_1, yielding $C_2 = 0.6 \times 10^{-19}$ F. The capacitance of the Au-NP/substrate junction is higher than that of the tip–NP junction because of the narrower spacing and the larger contact area in the former case.

Based on the orthodox theory and using the SETNETS program, the obtained fitting parameters are $R_1 = 0.1$ GΩ and $C_1 = 1.2 \times 10^{-19}$ F for the particle/substrate tunnel junction, $R_2 = 4.6$ GΩ and $C_2 = 0.6 \times 10^{-19}$ F for the particle–STM tip tunnel junction, and a fractional residual charge of $Q_0 = 0.05$e. The numerically fit curve is shown in Fig. 4(b), in which agreement with experimental data is achieved in the negative bias region, while the narrow Coulomb staircases causes a slight deviation of the fitting in the positive bias regime. The resistance of the Au particle–STM tip

Table 1
Electronic properties of junctions 1 and 2 in the DBTJ

Spectroscopy parameters	Electronic properties at junctions
Total capacitances from threshold voltage	$C_1 + C_2 = 0.18$ aF
Current slope of 30 pA/0.4 V and current jump of 100 pA	$R_2 \sim 8.9$ GΩ, $C_1 = 0.12$ aF, and $C_2 = 0.06$ aF
SET numerical fitting	$R_1 \sim 0.1$ GΩ, $R_2 \sim 4.6$ GΩ and $Q_0 = 0.05$e

junction is higher, because of the larger tunneling distance. Because the Coulomb gap is dominated by the larger capacitance in such two-junction systems (in our case, C_1 of the NP/substrate junction), the blockade width is independent of the current setpoint.

The resistance (R_1 of ~ 0.1 GΩ), or conductance ($1/R_1$), of junction 1 corresponds well with the resistance of alkanethiol molecules in a standing up configuration [5,23,24]. We note that this value is 1–2 orders of magnitude higher than previous reports [7,10]. In previous systems, lateral movement of the NPs and less than closely packed structures of the passivation layer likely led to a higher value of the measured molecular conductance. Our apparent resistance is consistent with Lindsay's work on a single octanedithiol molecule using a conducting AFM [5]. In his system, an individual Au-NP was used as an electrode to measure conductance of SAMs underneath and a charge resistance of 0.9 GΩ for octanedithiol was estimated [5]. Since no SET effects were observed in their work (supported by the lack of current blocking $\sim\pm 0.1$ V), it is possible that the Au-NPs fused with the Au tip while positioning and measuring conductance and merely function as electrodes. Despite differences in measuring and extracting the resistance for molecular conductance, some valuable comparison in R_1 can still be made. Clearly, charge injection from Au to the SAM is difficult due to the large energy barrier between the Au electrode and alkanethiols ($\sim$2.5 eV) [23]. Thus, both experiments measured tunneling resistance. Their resistance values of 0.1–0.9 GΩ are in close proximity to our R_1 of 0.1 GΩ for octanedithiols.

3.4. Single particle manipulation by STM

The spectroscopy measurements also facilitate the determination of single particle manipulation. The weakest link in the junction of Au-NPs/1, 8-octanedithiol molecules/Au(1 1 1) substrate is the S–Au bond with a binding energy of 1.8 eV, i.e., corresponding to a breakdown voltage of 1.8 V or an electric field of 1.9×10^9 V/m [20,27]. Thus, when the electric field on the junction of Au-NPs/1,8-octanedithiol molecules/Au(1 1 1)

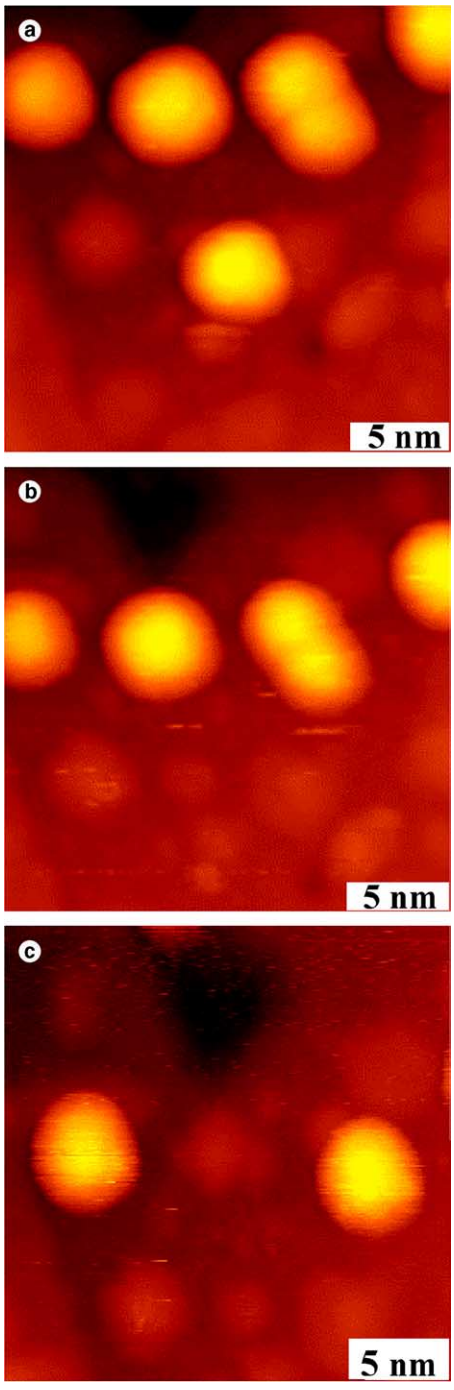

Fig. 5. STM manipulation of passivated Au nanoparticles. STM images before (a) and after the extraction of a single (b) and two Au NPs (c). The extraction was performed under the conditions of 0.3 V and 30 pA. The images were taken at 1.0 V and 30 pA.

substrate is below such a value, those immobilized NPs can be imaged without perturbation as shown in Fig. 2. When the S–Au bond between Au-NPs and Au(1 1 1) substrates is weakened by an increased electrical field, dissociation or desorption of the alkanethiol on Au starts to occur [20] and a single NP can be selectively detached and manipulated with nanometer precision and resolution.

The main steps for the NPs extraction are as follows: first, a single NP is selected by imaging the surface at a bias of ~1.0 V (electric field of $\sim 8 \times 10^8$ V/m). In the second step, the STM tip is parked above the selected NP, and the voltage is lowered below the charging voltage. Subsequently, the voltage is increased to ~1.8 V and the NP is extracted to the tip. In the final step, the NP can be deposited by applying an electrical pulse on the selected area. An example of the controlled extraction individual NPs shown in Fig. 5. Fig. 5(a) shows three NPs and a dimer surrounded by a decanethiol monolayer before manipulation. The tip was positioned above the single NP at the lower part of the image, and the bias voltage was then decreased to 0.3 V while the feedback was still active. When the bias voltage was increased to a value of 1.8 V, the NP was removed, as shown in Fig. 5(b). Repeating this procedure can remove one NP from the dimer, as shown in Fig. 5(c). It was also possible to remove NPs with a bias voltage of +1.0 V and 0.5 nA with a comparable success rate. Alternatively, the injection of a large current into the junction of Au-NPs/1, 8-octanedithiol molecules/Au(1 1 1) substrate could cause charge re-distribution along the S–Au bond as well, giving rise to the dissociation of alkanethiol adsorbates on either Au-NPs or the Au(1 1 1) substrate [20]. The NPs removed are often attached to the tip, which can be released after voltage pulsing with negative bias.

4. Conclusions

A surface science based, simple and reliable protocol has been developed to capture SET effects of metal NPs at room temperature. Particle immobilization on electrode surfaces are achieved using mixed alkanethiol and alkanedithiols, where alkanedithols attach NPs to Au electrodes. Subsequently, the rest of the gold surface is covered by an alkanethiol SAM. This approach of interfacial chemistry eliminates aggregation and the lateral motion of individual NPs under the STM probes, resulting in an accurate and reproducible imaging and I–V characterization. In addition, the surrounding decanethiol SAM provides an accurate reference for imaging and I–V measurements for NPs. The STM I–V spectroscopy studies clearly reveal the SET behavior at room temperatures, a large Coulomb gap (~1 eV) and fine Coulomb staircases (0.2–0.3 eV). Using the DBTJ model, one can quantify the electronic properties, e.g., resistance and capacitance, by curve fitting the equivalent circuit, as summarized in Table 1. In addition to nanoelectronics design, our approach provides a simple way for determining the threshold current and voltage under which individual Au-NPs may be detached and manipulated on surfaces.

Acknowledgments

The authors thank Dr. Jayne C. Garno and Mr. Christopher Fleming for scientific discussions. We appreciate the financial support from University of California, Davis, NSF (Grant CHE-0244830 and CHE0210807), and NIST (60NANB1D0072). Work at UCSC was supported by the National Science Foundation (CAREER Award CHE-0456130), the ACS-Petroleum Research Fund, and the University of California Santa Cruz. S.C. is a Cottrell Scholar of Research Corporation.

References

[1] E.S. Soldatov, S.P. Gubin, I.A. Maximov, G.B. Khomutov, V.V. Kolesov, A.N. Sergeev-Cherenkov, V.V. Shorokhov, K.S. Sulaimankulov, D.B. Suyatin, Microelectronic Engineering 69 (2003) 536.
[2] S.P. Gubin, Y.V. Gulayev, G.B. Khomutov, V.V. Kislov, V.V. Kolesov, E.S. Soldatov, K.S. Sulaimankulov, A.S. Trifonov, Nanotechnology 13 (2002) 185.
[3] A.C.R. Grayson, R.S. Shawgo, A.M. Johnson, N.T. Flynn, Y.W. Li, M.J. Cima, R. Langer, Proceedings of the IEEE 92 (2004) 6.
[4] M.A. Reed, Proceedings of the IEEE 87 (1999) 652.

[5] X.D. Cui, A. Primak, X. Zarate, J. Tomfohr, O.F. Sankey, A.L. Moore, T.A. Moore, D. Gust, G. Harris, S.M. Lindsay, Science 294 (2001) 571.
[6] J.W. Gerritsen, S.E. Shafranjuk, E.J.G. Boon, G. Schmid, H. van Kempen, Europhysics Letters 33 (1996) 279.
[7] T.P. Bigioni, L.E. Harrell, W.G. Cullen, D.E. Guthrie, R.L. Whetten, P.N. First, European Physical Journal D 6 (1999) 355.
[8] L.E. Harrell, T.P. Bigioni, W.G. Cullen, R.L. Whetten, P.N. First, Journal of Vacuum Science and Technology B 17 (1999) 2411.
[9] L.F. Chi, M. Hartig, T. Drechsler, T. Schwaack, C. Seidel, H. Fuchs, G. Schmid, Applied Physics A—Materials Science and Processing 66 (1998) S187.
[10] B. Wang, H.Q. Wang, H.X. Li, C.G. Zeng, J.G. Hou, X.D. Xiao, Physical Review B 63 (2001) 035403.
[11] K.K. Likharev, Proceedings of the IEEE 87 (1999) 606.
[12] R.P. Andres, T. Bein, M. Dorogi, S. Feng, J.I. Henderson, C.P. Kubiak, W. Mahoney, R.G. Osifchin, R. Reifenberger, Science 272 (1996) 1323.
[13] S.M. Goodnick, J. Bird, IEEE Transactions on Nanotechnology 2 (2003) 368.
[14] T. Fujisawa, T. Hayashi, Y. Hirayama, H.D. Cheong, Y.H. Jeong, Applied Physics Letters 84 (2004) 2343.
[15] N.K. Chaki, M. Aslam, T.G. Gopakumar, J. Sharma, R. Pasricha, I.S. Mulla, K. Vijayamohanan, Journal of Physical Chemistry B 107 (2003) 13567.
[16] P. Jiang, Z.F. Liu, S.M. Cai, Applied Physics Letters 75 (1999) 3023.
[17] H. Graf, J. Vancea, H. Hoffmann, Applied Physics Letters 80 (2002) 1264.
[18] S.W. Chen, Journal of Physical Chemistry B 104 (2000) 663.
[19] M. Brust, M. Walker, D. Bethell, D.J. Schiffrin, R. Whyman, Journal of the Chemical Society–Chemical Communications (1994) 801.
[20] G.H. Yang, G.Y. Liu, Journal of Physical Chemistry B 107 (2003) 8746.
[21] Y.L. Qian, G.H. Yang, J.J. Yu, T.A. Jung, G.Y. Liu, Langmuir 19 (2003) 6056.
[22] G.Y. Liu, S. Xu, Y.L. Qian, Accounts of Chemical Research 33 (2000) 457.
[23] D.M. Adams et al., Journal of Physical Chemistry B 107 (2003) 6668.
[24] E. Gomar-Nadal, G.K. Ramachandran, F. Chen, T. Burgin, C. Rovira, D.B. Amabilino, S.M. Lindsay, Journal of Physical Chemistry B 108 (2004) 7213.
[25] M.A. Rampi, O.J.A. Schueller, G.M. Whitesides, Applied Physics Letters 72 (1998) 1781.
[26] A.E. Hanna, M. Tinkham, Physical Review B 44 (1991) 5919.
[27] S.I. Khondaker, Z. Yao, L. Cheng, J.C. Henderson, Y.X. Yao, J.M. Tour, Applied Physics Letters 85 (2004) 645.